JOURNAL OF AIRCRAFT
Vol. 44, No. 6, November–December 2007

New Computational Procedure for Incorporating Computational Fluid Dynamics into Sonic Boom Prediction

Sriram K. Rallabhandi* and Dimitri N. Mavris†
Georgia Institute of Technology, Atlanta, Georgia 30332

DOI: 10.2514/1.32035

A new computational approach for the inclusion of computational fluid dynamics flow solutions into predicting sonic boom signatures is developed. Using existing computational fluid dynamics tools, a near-field flow solution is obtained over the surface of a computational cylinder a certain distance away from the aircraft's longitudinal axis. Near-field to far-field multipole-matching methodology is performed to calculate the corrected far field without calculating the multipole coefficients. The analytical derivation is provided and some results are presented and discussed.

Nomenclature

A_n	=	multipole distributions
F	=	Whitham F-function
F_n	=	near-field (uncorrected) Fourier component of the pressure cylinder
F_n^∞	=	far-field corrected Fourier component
$f_i(n)$	=	nth term in the expansion of the multipole function
G_n	=	g_n/g_∞
g_n	=	multipole function, order n
g_∞	=	far-field multipole function
K_i	=	ith dummy function used in simplification
M	=	Mach number
N	=	number of multipoles used
n	=	multipole order
p	=	pressure values over a computational fluid dynamics cylinder
R	=	radius of the computational fluid dynamics cylinder
r	=	radial coordinate
T	=	number of terms used in multipole expansion
x	=	axial coordinate
β	=	$\sqrt{M^2-1}$
γ	=	ratio of specific heats, 1.4
θ	=	azimuthal angle
κ	=	$\tau/2\beta r$
ξ	=	dummy variable
τ	=	$x-\beta r$

I. Introduction

WITH the ever-increasing power of computational resources, many researchers [1–5] are using computational fluid dynamics (CFD), advanced optimization, and multidisciplinary techniques in the conceptual and preliminary stages of aircraft design for sonic boom mitigation and shape optimization. CFD simulations have the ability to offer much more accurate analysis of the flowfield compared with the traditional linearized methods. If accurate sonic boom signatures at the ground level are desired, the ideal computational scenario would be to use CFD simulation all the way to the ground [6]. However, because this cannot be done in practical simulations, Page and Plotkin [7] provided an efficient method to incorporate CFD solutions for predicting sonic boom signatures on the ground. Using George's [8] multipole formulation, Page and Plotkin [7] showed that the solution of the perturbation potential equation using multipole formulation offers an elegant way to map the near-field results to their far-field counterparts. It has also been shown that if the extrapolation from near field to far field is not performed, the resulting ground signatures might not converge [9]. It is the belief of the authors that the numerical procedure suggested by Page and Plotkin [7] can be altered to provide new insights into the multipole-matching procedure, particularly because the implementation of their method is not available in the public domain. This forms the motivation for the present study.

Presented as Paper 3312 at the 24th AIAA Applied Aerodynamics Conference, San Francisco, CA, 5–8 June 2006; received 8 May 2007; revision received 18 June 2007; accepted for publication 1 July 2007.

*Research Engineer II, Aerospace Systems Design Lab. Member AIAA.
†Director and Boeing Professor of Advanced Aerospace Systems Analysis, Aerospace Systems Design Lab. Associate Fellow AIAA.

II. Background

Aircraft design for sonic boom reduction has received new life in recent years due to market demand [10,11] and a successful flight demonstration of the shaped sonic boom design philosophy [12]. With the renewed interest in this sector, many studies are being conducted to design aircraft for sonic boom reduction using nonlinear CFD analysis. Using CFD in sonic boom prediction involves computation of pressure at the interface between the CFD near field and acoustic far field. One of the methods used for this calculation was proposed and implemented by Page and Plotkin [7]. Their procedure starts the numerical analysis by using a general solution to the perturbation potential equation. Assuming lateral symmetry of the flowfield, the strength of the multipole distribution is obtained as shown in Eq. (1).

$$g_n(x,r) = -\frac{1}{2\pi}\frac{\cosh[n\cosh^{-1}(x/\beta r)]}{\sqrt{x^2-\beta^2 r^2}} \tag{1}$$

The CFD pressure field is Fourier-decomposed into n modes, with the corresponding Fourier components given in Eq. (2), where θ is the azimuthal ordinate, M is the freestream Mach number, γ is the ratio of specific heats, and p is the pressure over the CFD cylinder.

$$\begin{aligned} F_n(\tau,R) &= \frac{\sqrt{2\beta R}}{\gamma M^2}\frac{1}{2\pi}\int_0^{2\pi} p(\tau,\theta,R)\,\mathrm{d}\theta \qquad n=0 \\ F_n(\tau,R) &= \frac{\sqrt{2\beta R}}{\gamma M^2}\frac{1}{\pi}\int_0^{2\pi} p(\tau,\theta,R)\cos(n\theta)\,\mathrm{d}\theta \quad n\neq 0 \end{aligned} \tag{2}$$

The Fourier component corresponding to the CFD flowfield is given in terms of the multipole coefficients, as shown in Eq. (3), where ξ is the dummy integration variable and n is the same multipole order used in Eq. (2).

$$F_n(\tau, r) = \frac{1}{2\pi}\int_0^{\tau} \frac{A_n(\xi)}{\sqrt{\tau - \xi}} G_n(\tau - \xi, r)\, \mathrm{d}\xi \tag{3}$$

The objective is to use known distributions of F_n, as obtained from Eq. (2), to obtain a far-field approximation F_n^{∞}, as shown in Eq. (4). This far-field approximation represents a solution sufficiently far away from the aircraft so that the three-dimensional crossflow effects near the aircraft are resolved. This is done so that ray-theory-based acoustic propagation analysis can be used based on the axisymmetric-equivalent-body method presented originally by Whitham [13].

$$F_n^{\infty}(\tau) = \frac{1}{2\pi}\int_0^{\tau} \frac{A_n(\xi)}{\sqrt{\tau - \xi}}\, \mathrm{d}\xi \tag{4}$$

Page and Plotkin [7] suggest using a numerical procedure to solve for multipole distributions A_n using Eqs. (2) and (3) and then using these distributions to obtain the corrected far field using Eq. (4). Following along similar lines, Lyman and Morgenstern [14] claim to have obtained the corrected far field to a multipole order of 11. In the following sections, it is shown mathematically that the far-field Fourier component F_n^{∞} can be obtained directly from its near-field counterpart F_n without having to calculate the multipole distributions.

III. Mathematical Formulation of the Proposed Method

A. Derivation of the Strength of the Multipole Distribution

Using $\tau = x - \beta r$, the nonconstant denominator term in Eq. (1) is expanded as follows:

$$x^2 - \beta^2 r^2 = \tau^2 + 2\beta r\tau = 2\beta r\tau\left(\frac{\tau}{2\beta r} + 1\right) \tag{5}$$

Using the preceding substitution, the denominator term in Eq. (1) is written as

$$\frac{1}{\sqrt{x^2 - \beta^2 r^2}} = \frac{1}{\sqrt{2\beta r\tau}}\frac{1}{\sqrt{\kappa + 1}} \tag{6}$$

where $\kappa = \tau/2\beta r$. Invoking the inverse hyperbolic identity, the interior term in the numerator of Eq. (1) is written as in Eq. (7).

$$\cosh^{-1}\frac{x}{\beta r} = \sinh^{-1}\sqrt{\left(\frac{x}{\beta r}\right)^2 - 1} \tag{7}$$

Equation (7) is recast in terms of κ, as given in Eq. (8).

$$\cosh^{-1}\frac{x}{\beta r} = \sinh^{-1}\sqrt{\left(\frac{x}{\beta r}\right)^2 - 1} = \sinh^{-1}\sqrt{4\kappa(\kappa + 1)} \tag{8}$$

Inverse hyperbolic expansions render the hyperbolic cosine term in Eq. (1), as given in Eq. (9).

$$\cosh\left[n\cosh^{-1}\left(\frac{x}{\beta r}\right)\right] = 1 + 2n^2\kappa + \left(\frac{2n^4}{3} - \frac{2n^2}{3}\right)\kappa^2 + \left(\frac{16n^2}{45} - \frac{4n^4}{9} + \frac{4n^6}{45}\right)\kappa^3 + \cdots \tag{9}$$

Putting both denominator and numerator together in expression (1) and simplifying yields Eq. (10) for the general expression of the nth-order multipole g_n.

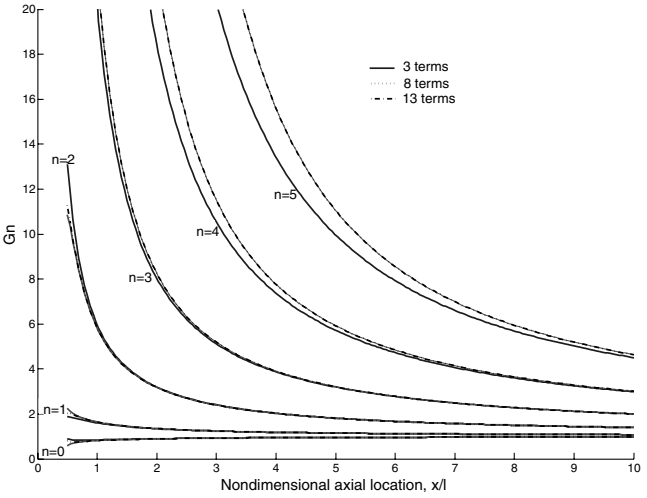

Fig. 1 Comparison of multipole function expanded to varying terms.

$$g_n(x, r) = -\frac{1}{2\pi}\frac{1}{\sqrt{2\beta r\tau}}\left[1 + \left(n^2 - \frac{1}{4}\right)\left(\frac{\tau}{\beta r}\right) + \left(\frac{16n^4 - 40n^2 + 9}{96}\right)\left(\frac{\tau}{\beta r}\right)^2 + \left(\frac{64n^6 - 560n^4 + 1036n^2 - 225}{5760}\right)\left(\frac{\tau}{\beta r}\right)^3 + \cdots\right] \tag{10}$$

This expression can be split into two components, as shown in Eq. (11). The first term, g_{∞}, corresponds to the $1/\sqrt{r}$ far-field dependence, independent of n, whereas the second term, G_n, is responsible for three-dimensional crossflow effects. The terms $f_i(n)$ in Eq. (12) are obtained by expanding the combination of the hyperbolic cosine term in Eq. (9) and the denominator term in Eq. (6) to the required number of terms, $T + 1$. The expressions for some $f_i(n)$ terms are provided in Appendix A.

Figure 1 depicts the expression (12) for successive multipole orders $n = 0, \ldots, 5$, using an increasing number of terms in the approximation, as a function of the nondimensional body lengths away from the aircraft longitudinal axis. It is seen that for the lower-order multipoles, using a three- or eight-term approximation is inferior to the 13-term approximation; however, as the order of the multipoles increases, an eight-term approximation is sufficiently accurate. Also observed from this plot is the fact that as the distance behind the body increases, each of the multipole terms proceeds to a value of 1 asymptotically. Furthermore, the rate of convergence to the asymptotic limit of the higher-order multipoles is greater than their lower-order counterparts. In this study, the final results are calculated using a 13-term approximation [i.e., the first constant term and $12 f_i(n)$ $(i = 0, \ldots, 11)$ terms].

$$g_n(\tau, r) = g_{\infty}(\tau, r) G_n(\tau, r) \tag{11}$$

where

$$G_n(\tau, r) = 1 + \sum_{i=0}^{T-1} f_i(n)\left(\frac{\tau}{\beta r}\right)^{i+1} + O((\tau)^{T+1}) \tag{12}$$

and

$$g_{\infty}(\tau, r) = -\frac{1}{2\pi}\frac{1}{\sqrt{2\beta r\tau}} \tag{13}$$

Substituting Eq. (12), with variables changed to $(\tau\text{-}\xi, R)$, into the uncorrected Fourier component of the F-function from Eq. (3) results in Eq. (14) after expanding and rearranging the terms.

$$F_n(\tau,R)=\left[1+\sum_{i=0}^{T-1}f_i(n)\left(\frac{\tau}{\beta R}\right)^{i+1}\right]F_n^{\infty}(\tau)$$
$$-\left[\sum_{i=0}^{T-1}\frac{f_i(n)}{\beta R}\left(\frac{\tau}{\beta R}\right)^{i}\binom{i+1}{1}\right]\int_0^{\tau}\xi\frac{A_n(\xi)}{\sqrt{(\tau-\xi)}}\mathrm{d}\xi$$
$$+\left[\sum_{i=1}^{T-1}\frac{f_i(n)}{(\beta R)^2}\left(\frac{\tau}{\beta R}\right)^{i-1}\binom{i+1}{2}\right]\int_0^{\tau}\xi^2\frac{A_n(\xi)}{\sqrt{(\tau-\xi)}}\mathrm{d}\xi\cdots(-1)^T\frac{f_{T-1}(n)}{(\beta R)^T}$$
$$\times\int_0^{\tau}\xi^T\frac{A_n(\xi)}{\sqrt{(\tau-\xi)}}\mathrm{d}\xi \tag{14}$$

The solution strategy is to break up each of the integral terms in Eq. (14) by performing integration by parts. The procedure builds upon the relations provided in Eqs. (3) and (4). Let us assume a function for the indefinite integral in Eq. (15), where K_i is the ith dummy function used in the analytical simplification. The existence of this integral is guaranteed based on the existence of F_n^{∞}.

$$\int\frac{A_n(\xi)}{\sqrt{\tau-\xi}}\,\mathrm{d}\xi=K_1(\xi) \tag{15}$$

Using the indefinite integral function and imposing the limit values yields Eq. (16), relating the unknown indefinite integral to the far-field Fourier component. Rearranging the terms leads to Eq. (17).

$$\int_0^{\tau}\frac{A_n(\xi)}{\sqrt{\tau-\xi}}\,\mathrm{d}\xi=K_1(\tau)-K_1(0)=F_n^{\infty}(\tau) \tag{16}$$

$$K_1(\tau)=K_1(0)+F_n^{\infty}(\tau) \tag{17}$$

Consider the integral portion of the second term, which is simplified as given in Eq. (18), using the indefinite integral in Eq. (15).

$$\int_0^{\tau}\xi\frac{A_n(\xi)}{\sqrt{(\tau-\xi)}}\,\mathrm{d}\xi=\tau K_1(\tau)-\int_0^{\tau}K_1(\xi)\,\mathrm{d}\xi \tag{18}$$

Using Eq. (17), Eq. (18) is expanded as in Eq. (19).

$$\int_0^{\tau}\xi\frac{A_n(\xi)}{\sqrt{(\tau-\xi)}}\,\mathrm{d}\xi=\tau[F_n^{\infty}(\tau)+K_1(0)]-\int_0^{\tau}[F_n^{\infty}(\xi)+K_1(0)]\,\mathrm{d}\xi \tag{19}$$

Equation (19) becomes Eq. (20) after the terms involving $K_1(0)$ drop out.

$$\int_0^{\tau}\xi\frac{A_n(\xi)}{\sqrt{(\tau-\xi)}}\,\mathrm{d}\xi=\tau F_n^{\infty}(\tau)-\int_0^{\tau}F_n^{\infty}(\xi)\,\mathrm{d}\xi \tag{20}$$

Let the indefinite integral of $K_1(\xi)$ be as given in Eq. (21).

$$\int K_1(\xi)\,\mathrm{d}\xi=K_2(\xi) \tag{21}$$

Using Eq. (17), Eq. (21) is written as

$$\int K_1(\xi)\,\mathrm{d}\xi=\int F_n^{\infty}(\xi)\,\mathrm{d}\xi+K_1(0)\xi=K_2(\xi) \tag{22}$$

Using the definite integral, with limits as specified in Eq. (14), Eq. (23) is obtained.

$$\int_0^{\tau}K_1(\xi)\,\mathrm{d}\xi=\int_0^{\tau}F_n^{\infty}(\xi)\,\mathrm{d}\xi+K_1(0)\tau=K_2(\tau)-K_2(0) \tag{23}$$

Shifting terms between the left- and right-hand sides of Eq. (23), Eq. (24) is obtained to give the unknown function $K_2(\tau)$ in terms of F_n^{∞}.

$$K_2(\tau)=\int_0^{\tau}F_n^{\infty}(\xi)\,\mathrm{d}\xi+K_1(0)\tau+K_2(0) \tag{24}$$

Using Eq. (21), the integral portion of the third term in Eq. (14) becomes the following.

$$\int_0^{\tau}\xi^2\frac{A_n(\xi)}{\sqrt{(\tau-\xi)}}\,\mathrm{d}\xi=\tau^2K_1(\tau)-2\tau K_2(\tau)+2\int_0^{\tau}K_2(\xi)\,\mathrm{d}\xi \tag{25}$$

Using Eqs. (17) and (24), Eq. (25) is simplified to

$$\int_0^{\tau}\xi^2\frac{A_n(\xi)}{\sqrt{(\tau-\xi)}}\,\mathrm{d}\xi$$
$$=\tau^2F_n^{\infty}(\tau)-2\tau\int_0^{\tau}F_n^{\infty}(\xi)\,\mathrm{d}\xi+2\int_0^{\tau}\int_0^{\xi_1}F_n^{\infty}(\xi)\,\mathrm{d}\xi\,\mathrm{d}\xi_1 \tag{26}$$

Continuing along similar lines, Eqs. (27) and (28) can be obtained for the third and fourth integrals in Eq. (14). A clear pattern in the expressions for these integrals can be observed. A generalization of these is provided in Eq. (29). According to this generalized formula, the integral terms in Eq. (14) can be recast as integral terms of the far-field corrected Fourier component for any number of terms desired.

$$\int_0^{\tau}\xi^3\frac{A_n(\xi)}{\sqrt{(\tau-\xi)}}\,\mathrm{d}\xi=\tau^3F_n^{\infty}(\tau)-3\tau^2\int_0^{\tau}F_n^{\infty}(\xi)\,\mathrm{d}\xi$$
$$+6\tau\int_0^{\tau}\int_0^{\xi}F_n^{\infty}(\xi_1)\,\mathrm{d}\xi_1\,\mathrm{d}\xi-6\int_0^{\tau}\int_0^{\xi}\int_0^{\xi_1}F_n^{\infty}(\xi_2)\,\mathrm{d}\xi_2\,\mathrm{d}\xi_1\,\mathrm{d}\xi \tag{27}$$

$$\int_0^{\tau}\xi^4\frac{A_n(\xi)}{\sqrt{(\tau-\xi)}}\,\mathrm{d}\xi$$
$$=\tau^4F_n^{\infty}(\tau)-4\tau^3\int_0^{\tau}F_n^{\infty}(\xi)\,\mathrm{d}\xi+12\tau^2\int_0^{\tau}\int_0^{\xi}F_n^{\infty}(\xi_1)\,\mathrm{d}\xi_1\,\mathrm{d}\xi$$
$$-24\tau\int_0^{\tau}\int_0^{\xi}\int_0^{\xi_1}F_n^{\infty}(\xi_2)\,\mathrm{d}\xi_2\,\mathrm{d}\xi_1\,\mathrm{d}\xi$$
$$+24\int_0^{\tau}\int_0^{\xi}\int_0^{\xi_1}\int_0^{\xi_2}F_n^{\infty}(\xi_3)\,\mathrm{d}\xi_2\,\mathrm{d}\xi_3\,\mathrm{d}\xi_1\,\mathrm{d}\xi \tag{28}$$

$$\int_0^{\tau}\xi^T\frac{A_n(\xi)}{\sqrt{(\tau-\xi)}}\,\mathrm{d}\xi=\tau^TF_n^{\infty}(\tau)-T\tau^{T-1}\int_0^{\tau}F_n^{\infty}(\xi)\,\mathrm{d}\xi$$
$$+T(T-1)\tau^{T-2}\int_0^{\tau}\int_0^{\xi}F_n^{\infty}(\xi_1)\,\mathrm{d}\xi_1\,\mathrm{d}\xi\cdots$$
$$+(-1)^{T+1}(T!)\int_0^{\tau}\int_{(T-1)\text{times}}\cdots\int F_n^{\infty}(\xi_{T-1})\,\mathrm{d}\xi_{T-1}\cdots\mathrm{d}\xi_1\,\mathrm{d}\xi \tag{29}$$

Inserting these equations into Eq. (14) and simplification leads to an expression relating the uncorrected Fourier component $F_n(\tau,R)$ and the far-field corrected Fourier component $F_n^{\infty}(\tau)$, as given in Eq. (30). This shows that the corrected Fourier component may be obtained from the uncorrected counterpart by solving the Tth-order integral equation for each multipole order represented by n.

$$F_n(\tau,R)=F_n^{\infty}(\tau)$$
$$+\sum_{i=0}^{T-1}f_i(n)(i+1)!\int_{0(i+1)\text{times}}^{\tau}\cdots\int_0^{\xi_i}F_n^{\infty}(\xi_i)\,\mathrm{d}\xi_i\cdots\mathrm{d}\xi_1 \tag{30}$$

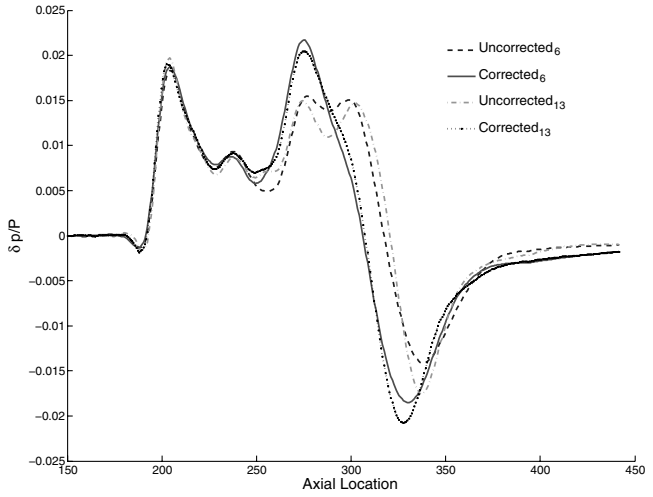

Fig. 2 Comparison of corrected and uncorrected signatures using 6 and 13 multipoles.

B. Solution Procedure for Obtaining the Corrected Fourier Component

Let us represent a dummy function y as in Eq. (31).

$$y = \int_{0(T)\text{times}}^{\tau} \cdots \int_{0}^{\xi_T} F_n^{\infty}(\xi_T)\,\mathrm{d}\xi_T \cdots \mathrm{d}\xi_1 \tag{31}$$

Under the preceding definition, Eq. (30) becomes a Tth-order ordinary differential equation, as shown in Eq. (32). This equation can be split into a system of T first-order differential equations and solved simultaneously using a differential equation solver. Boundary conditions need to be specified to solve for the ODE system. In this case, the boundary conditions that need to be specified are the successive integrals of the corrected Fourier component at the first axial location, which can be set to zero. Once the solution of the ODE system is obtained, the corrected Fourier component can be calculated in a straightforward manner. An example solution procedure for $T = 5$ is provided in Appendix B.

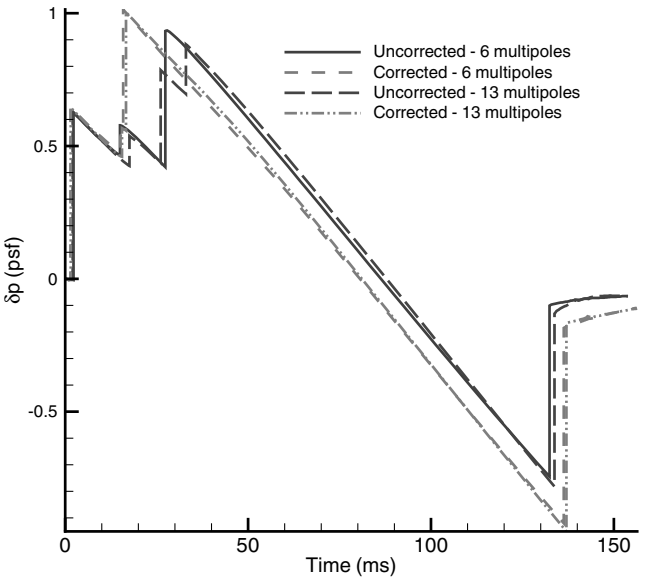

Fig. 4 Ground pressure signature comparison for configuration 1.

$$F_n(\tau, R) = y^{(T)} + \sum_{i=0}^{T-1} f_i(n)(i+1)!\,y^{(T-1-i)} \tag{32}$$

Finally, the computed Fourier component of the corrected F-function, F_n^{∞}, is used to compute the actual F-function F to be supplied to the acoustic propagation scheme, as given in Eq. (33), where N is the number of multipoles used.

$$F(\tau, \theta) = \sum_{n=0}^{N-1} F_n^{\infty}(\tau)\cos(n\theta) \tag{33}$$

IV. Results

In this section, results obtained over two arbitrary configurations are presented and discussed.

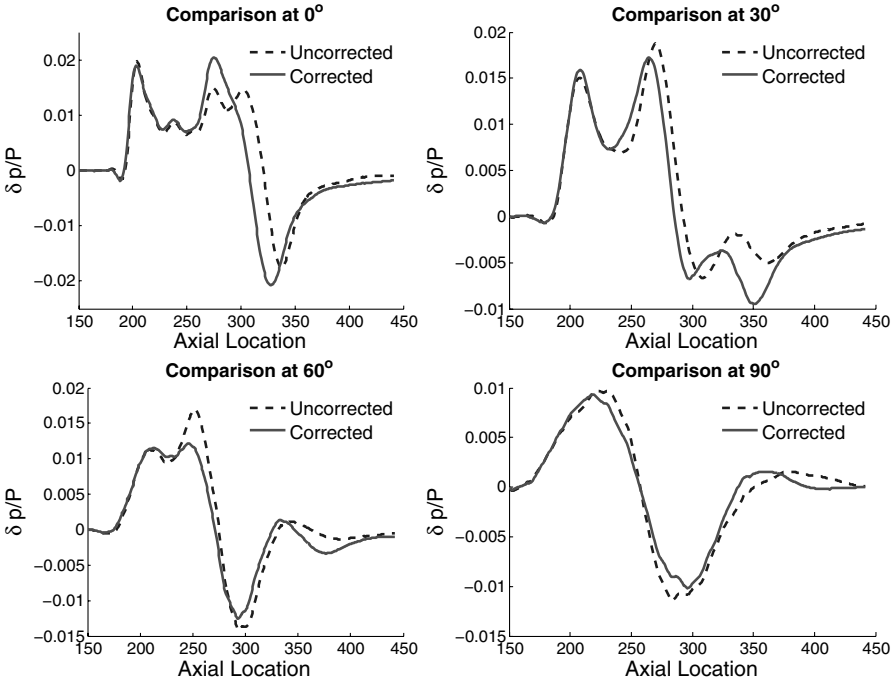

Fig. 3 Azimuthal comparison of corrected and uncorrected signatures using 13 multipoles.

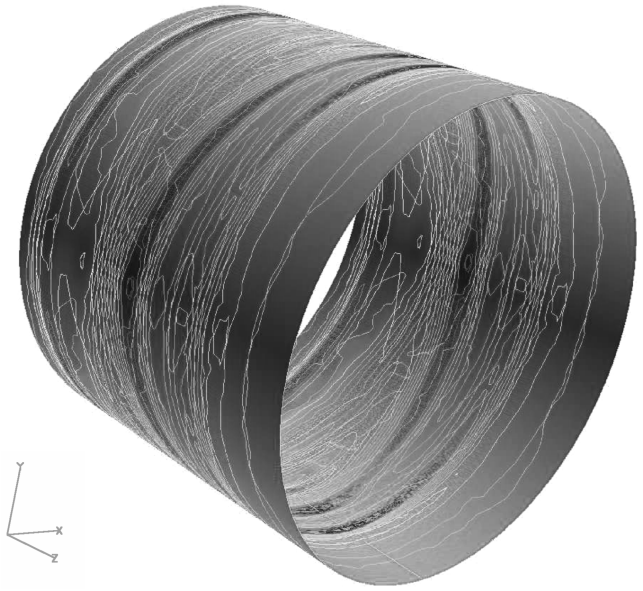

Fig. 5 CFD cylinder pressure contours for configuration 2.

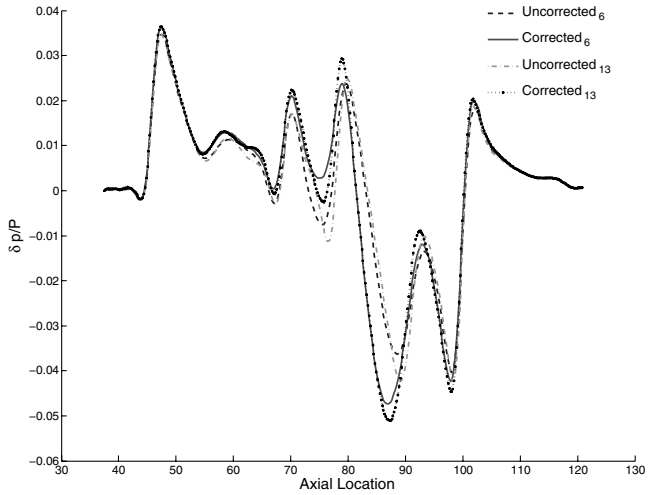

Fig. 6 Near-field signature comparison using different multipoles for configuration 2.

A. Example Case 1

To demonstrate the proposed approach, CFD cylindrical pressure data are obtained around an arbitrary aircraft (configuration 1) [15] with a length of 120 ft for a freestream Mach number of 120 ft and an altitude of 50,000 ft. Following the derivation given in the previous sections, the Fourier components of the near-field signature and the corresponding far-field corrected signature are computed.

After the computation of several multipole far-field Fourier components, they are azimuthally summed together to obtain the actual F-function to be supplied to the acoustic propagation program. Figure 2 compares the corrected and uncorrected components of the undertrack F-function using 6 and 13 multipoles, shown as subscripts in the legend, both using 13 terms in the G_n expansion. A 12th-order ODE, broken into a system of 12 first-order ODEs, is solved. Comparing the uncorrected and corrected versions, it is seen that because of the multipole correction, the magnitude of the peaks is increased in the undertrack signature and flat regions are removed due to azimuthal averaging. Increasing the number of multipoles to 13, causes additional correction in the form of expansion in the midsection of the signature (between axial locations 285 and 315), reduced magnitude ahead of this expansion, and increased magnitude rear of it. This shows that using six multipoles is not sufficient to obtain converged far-field correction results for this configuration. Comparison of these two shows that additional multipoles resolve the higher-order diffraction effects. As the number of multipoles is increased, the accuracy of the correction is improved. However, due to the decreasing multiplication factors for higher-order multipoles, the effect on the correction gradually decreases.

The comparison between the uncorrected and far-field corrected pressure signatures at different azimuthal angles is depicted in Fig. 3. It is seen that the corrected signature along the undertrack (0 deg) is larger in magnitude than the uncorrected signature, whereas the opposite is true as the azimuth angle proceeds toward more lateral (90 deg) angles. This is explained as being caused by the diffraction of lift.

Having obtained the corrected far-field F-function distributions, the modified Thomas waveform parameter method [16] included within PCBoom [17] is used to calculate the ground pressure signatures. Figure 4 provides the comparison of the ground pressure signatures using 6 and 13 multipoles, along with computed signatures, without performing the far-field correction. First, it is seen that if the CFD pressure is not corrected, then the resulting ground signature has signature duration, shock strengths, and magnitudes very different from their corrected counterparts. This kind of behavior has been observed in the past. Observation of the corrected ground signature using 6 and 13 multipoles reveals that

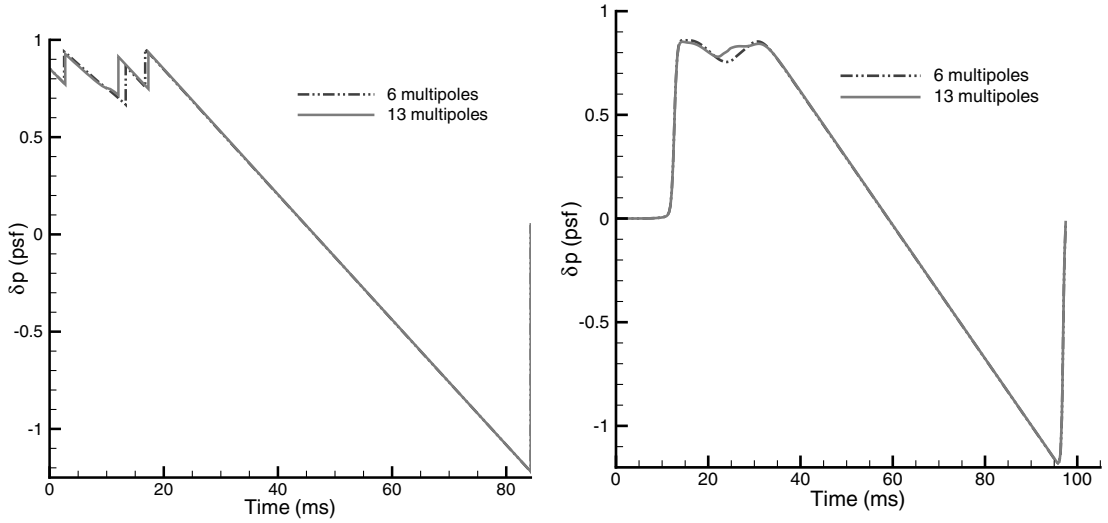

a) Zero rise time **b) Tangent hyperbolic rise time**

Fig. 7 Sonic boom ground signature comparison using 13 multipoles for configuration 2.

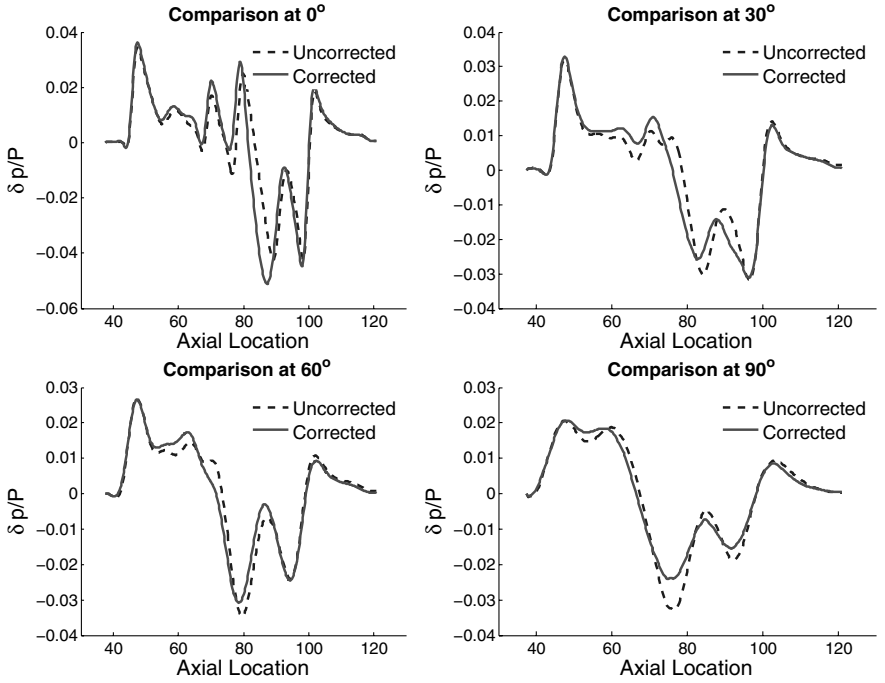

Fig. 8 Comparison between uncorrected and corrected signatures using 13 multipoles.

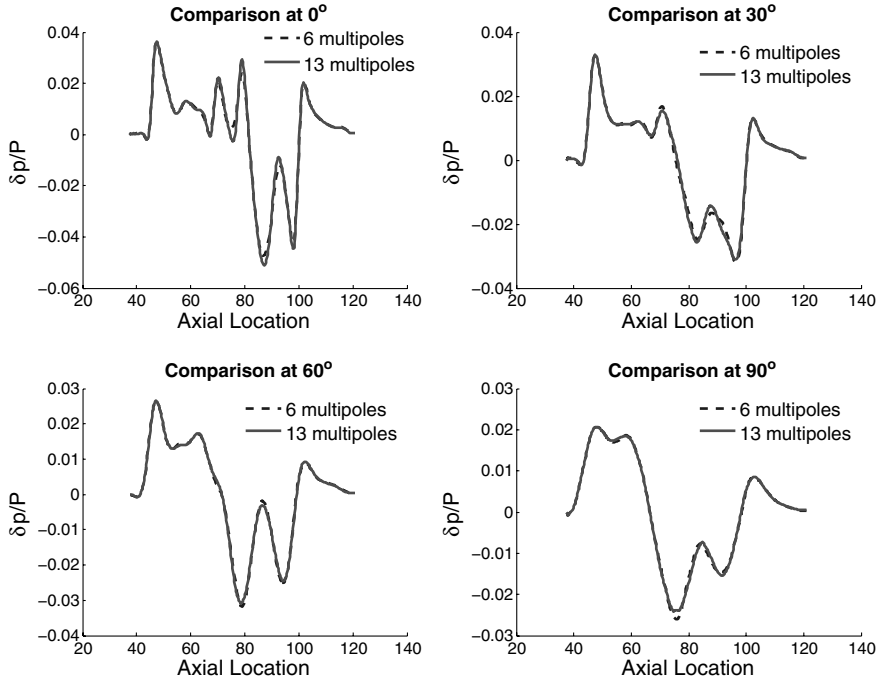

Fig. 9 Comparison between corrected signatures using 6 and 13 multipoles.

considering more multipoles has two effects. First, the shock magnitudes are slightly reduced and, more important, the rate of expansion is more pronounced when more multipoles are used for this configuration.

B. Example Case 2

The proposed CFD matching methodology is used to compare the uncorrected and corrected signatures for a second configuration (configuration 2). The CFD cylinder showing the pressure contours for this geometry is depicted in Fig. 5 for a flowfield Mach number of 1.4.

Figure 6 depicts the corrected and uncorrected undertrack pressure signatures using 6 and 13 multipoles. It is observed that the corrected signatures have larger magnitude and are shifted left when compared with their uncorrected counterparts. Consideration of 13 multipoles causes the corrected signature shape to vary at multiple locations. It shows that prematurely truncating the multipole order can affect the pressure signature predicted on the ground. It is observed that this configuration has a higher initial shock followed by smaller shocks from other aircraft components. Therefore, from the sonic boom minimization theory, one could predict that the sonic boom footprint of this configuration is going to be less intense. Because the sonic boom signature on the ground is extremely sensitive to the starting pressure signature, it is important to include several multipoles in the multipole-matching procedure, particularly for low-boom configurations. Additional comparisons using a lower or higher number of terms can also be plotted to show the sensitivity of the results to the

number of terms used, however, that is excluded here for brevity. Using 13 terms was sufficient for the cases considered in this study.

The ground pressure signatures obtained using 6 and 13 multipoles over the CFD pressure cylinder of configuration 2 is depicted in Fig. 7. Figure 7a shows that the duration of the signature and the shock magnitudes are comparable, but the shock locations are different because of the extent and location of the compression and expansion regions in the near-field corrected signature. Figure 7b shows the ground signature comparison using a tangent hyperbolic rise time correction, assuming a 1-ms rise time for a shock pressure jump of 1 psf. It is seen that using 13 multipoles produces a signature that is closer to a flat-top signature than using six multipoles. This also substantiates our claim from the previous paragraph that this configuration is a low-boom design.

The comparison between the uncorrected and far-field corrected pressure signatures at various azimuthal angles is depicted in Fig. 8. As observed before, the corrected signature along the undertrack (0 deg) is larger in magnitude than the uncorrected signature, whereas the opposite is true as the azimuth angle become more lateral (90 deg). Finally, Fig. 9 depicts the comparison between far-field corrected signatures using 6 and 13 multipoles at different azimuthal angles. It is seen that the effect of increasing multipoles decreases as the lateral angle increases.

Using the proposed computational strategy, the pressure field from the CFD solver can be mapped to an equivalent far-field signature that corrects the near-field signature to any desired multipole order and to the desired number of multipole function approximation terms.

V. Conclusions

A new computational procedure for the near-field to far-field matching procedure was developed and implemented. This method offers an elegant and efficient method to calculate corrected far-field F-functions for extrapolation of CFD signatures to any desired multipole order. The analytical derivation and the solution using ordinary differential equations provides a new insight into solving the matching problem. The approach presented is easily implemented in a computer. Other schemes for carrying out the multipole-matching procedure are not available in the public domain. The proposed procedure may need to be compared with those schemes to test for accuracy and computational cost.

Appendix A: Expansions of Multipole Functions

$$f_0(n) = n^2 - \tfrac{1}{4} \tag{A1}$$

$$f_1(n) = \frac{16n^4 - 40n^2 + 9}{96} \tag{A2}$$

$$f_2(n) = \frac{64n^6 - 560n^4 + 1036n^2 - 225}{5760} \tag{A3}$$

$$f_3(n) = \left[\frac{35}{128} - \frac{3229n^2}{2520} + \frac{141n^4}{180} - \frac{6n^6}{45} + \frac{2n^8}{315}\right]\frac{1}{16} \tag{A4}$$

$$f_4(n) = \left[\frac{-63}{256} + \frac{117469n^2}{100800} - \frac{51843n^4}{68040} + \frac{209n^6}{1350} - \frac{11n^8}{945} + \frac{4n^{10}}{14175}\right]\frac{1}{32} \tag{A5}$$

$$f_5(n) = \left[\frac{231}{1024} - \frac{1021391n^2}{950400} + \frac{1997021n^4}{2721600} - \frac{28067n^6}{170100} + \frac{871n^8}{56700} - \frac{26n^{10}}{42525} + \frac{4n^{12}}{467775}\right]\frac{1}{64} \tag{A6}$$

$$f_6(n) = \left[\frac{-429}{2048} + \frac{2430898831n^2}{2421619200} - \frac{1206053n^4}{1710720} + \frac{218347n^6}{1360800} - \frac{11911n^8}{170100} + \frac{11n^{10}}{12150} - \frac{2n^{12}}{93555} + \frac{8n^{14}}{42567525}\right]\frac{1}{128} \tag{A7}$$

$$f_7(n) = \left[\frac{6435}{32768} - \frac{60997921n^2}{64576512} + \frac{24615717239n^4}{36324288000} - \frac{15313957n^6}{89812800} + \frac{5599613n^8}{285768000} - \frac{4097n^{10}}{3572100} + \frac{493n^{12}}{14033250} - \frac{68n^{14}}{127702575} + \frac{2n^{16}}{638512875}\right]\frac{1}{256} \tag{A8}$$

$$f_8(n) = \left[\frac{-12155}{65536} + \frac{141433003757n^2}{158083301376} - \frac{426540447313n^4}{653837184000} + \frac{249938765093n^6}{1471133664000} - \frac{391080857n^8}{18860688000} + \frac{574123n^{10}}{428652000} - \frac{85177n^{12}}{1768189500} + \frac{1843n^{14}}{1915538625} - \frac{19n^{16}}{1915538625} + \frac{4n^{18}}{97692469875}\right]\frac{1}{512} \tag{A9}$$

$$f_9(n) = \left[\frac{46189}{262144} - \frac{25587296781661n^2}{30035827261440} + \frac{79923511502753n^4}{127031224320000} - \frac{164181914927n^6}{980755776000} + \frac{316100258731n^8}{14711336640000} - \frac{2008213n^{10}}{1347192000} + \frac{604841n^{12}}{10103940000} - \frac{16333n^{14}}{11493231750} + \frac{107n^{16}}{5472967500} - \frac{2n^{18}}{13956067125} + \frac{4n^{20}}{9280784638125}\right]\frac{1}{1024} \tag{A10}$$

$$f_{10}(n) = [-0.168188 + 0.814695n^2 - 0.6079416n^4 + 0.166066n^6 - 0.021967n^8 + 0.001609n^{10} - 7.0047 \times 10^{-5}n^{12} + 1.87478 \times 10^{-6}n^{14} - 3.0965 \times 10^{-8}n^{16} + 3.0606 \times 10^{-10}n^{18} - 1.6521 \times 10^{-12}n^{20} + 3.7315 \times 10^{-15}n^{22}]\frac{1}{2048} \tag{A11}$$

$$f_{11}(n) = [0.16118 - 0.7819n^2 + 0.5885n^4 - 0.16355n^6 + 0.02225n^8 - 0.0017n^{10} + 7.8787 \times 10^{-5}n^{12} - 2.3042 \times 10^{-6}n^{14} + 4.3261 \times 10^{-8}n^{16} - 5.117 \times 10^{-10}n^{18} + 3.8011 \times 10^{-12}n^{20} - 1.5548 \times 10^{-14}n^{22} + 2.704 \times 10^{-17}n^{24}]\frac{1}{4096} \tag{A12}$$

Appendix B: ODE System for $T = 5$

When expression (12) is truncated at $T = 5$, the resulting ODE is given in Eq. (B1), using the definition provided in Eq. (31).

$$y^{(5)} + \frac{f_0(n)}{\beta R}y^{(4)} + \frac{2f_1(n)}{(\beta R)^2}y^{(3)} + \frac{6f_2(n)}{(\beta R)^3}y^{(2)} + \frac{24f_3(n)}{(\beta R)^4}y^{(1)} + \frac{120f_4(n)}{(\beta R)^5}y = F_n(\tau, R) \tag{B1}$$

The preceding equation can be solved as a system of first-order ODEs, as given in Eq. (B2).

$$y^{(1)} = y_2 \qquad y_2^{(1)} = y_3 \qquad y_3^{(1)} = y_4 \qquad y_4^{(1)} = y_5$$
$$y_5^{(1)} + \frac{f_0(n)}{\beta R} y_5 + \frac{2f_1(n)}{(\beta R)^2} y_4 + \frac{6f_2(n)}{(\beta R)^3} y_3 + \frac{24f_3(n)}{(\beta R)^4} y_2 + \frac{120f_4(n)}{(\beta R)^5} y = F_n(\tau, R) \tag{B2}$$

The solution of the ODE system provides the solution vector $[y, y_2, y_3, y_4, y_5]$. $F_n^{\infty}(\tau)$ is given by $y_5^{(1)}$. Therefore, the corrected Fourier component is obtained by using the solution vector and the final equation of the ODE system.

Acknowledgments

This work was supported in part by NASA Langley Research Center grant 1606Y28 titled "Next Generation Conceptual Design Tools for the Nation Future Air Transportation Network" with Craig Nickol and Neil Kuhn acting as technical monitors. The authors would like to acknowledge the receipt of computational fluid dynamics (CFD) cylinder data for all the configurations from Neil Kuhn. We would also like to thank Kamran Fouladi and Dave Graham for providing access to the CFD cylinder data.

References

[1] Miles, R. B., Martinelli, L., Macheret, S. O., Shneider, M., Girgis, I. G., Zaidi, S. H., Mansfield, D. K., Siclari, M., Smereczniak, P., Kashuba, R., and Vogel, P., "Suppression of Sonic Boom by Dynamic Off-Body Energy Addition and Shape Optimization," AIAA Paper 2002-150, Jan. 2002.

[2] Nadarajah, S., Jameson, A., and Alonso, J., "Sonic Boom Reduction Using an Adjoint Method for Wing-Body Configurations in Supersonic Flow," AIAA Paper 2002-5547, Sept. 2002.

[3] Chung, H.-S., Choi, S., and Alonso, J., "Supersonic Business Jet Design Using Knowledge-Based Genetic Algorithm with Adaptive, Unstructured Grid Methodology," AIAA Paper 2003-3791, June 2003.

[4] Sasaki, D., and Obayashi, S., "Low-Boom Design Optimization for SST Canard-Wing-Fuselage Configuration," AIAA Paper 2003-3432, June 2003.

[5] Farhat, C., Maute, K., Argrow, B., and Nikbay, M., "A Shape Optimization Methodology for Reducing the Sonic Boom Initial Pressure Rise," AIAA Paper 2002-145, Jan. 2002.

[6] Kandil, O. A., Yang, Z., and Bobbitt, P. J., "Prediction of Sonic Boom Signature Using Euler-Full Potential CFD with Grid Adaptation and Shock Fitting," AIAA Paper 2002-2542, June 2002.

[7] Page, J. A., and Plotkin, K. J., "An Efficient Method for Incorporating Computational Fluid Dynamics into Sonic Boom Prediction," AIAA Paper 91-3275, Sept. 1991.

[8] George, A., "Reduction of Sonic Boom by Azimuthal Redistribution of Overpressure," AIAA Paper 68-159, Jan. 1968.

[9] Plotkin, K. K., and Page, J. A., "Extrapolation of Sonic Boom Signatures from CFD Solutions," AIAA Paper 2002-922, Jan. 2002.

[10] Darden, C. M., "The Importance of Sonic Boom Research in the Development of Future High Speed Aircraft," *Journal of the National Technical Association*, Vol. 65, No. 3, 1992, pp. 54–62.

[11] Henne, P. A., "Case for Small Supersonic Civil Aircraft," *Journal of Aircraft*, Vol. 42, No. 3, 2005, pp. 765–774.

[12] Pawlowski, J. W., Graham, D. H., Boccadoro, C. H., Coen, P. G., and Maglieri, D. J., "Origins and Overview of the Shaped Sonic Boom Demonstration Program," AIAA Paper 2005-5, Jan. 2005.

[13] Whitham, G., "The Flow Pattern of a Supersonic Projectile," *Communications on Pure and Applied Mathematics*, Vol. 5, 1952, pp. 301–347. doi:10.1002/cpa.3160050305

[14] Lyman, V., and Morgenstern, J. M., "Calculated and Measured Pressure Fields for an Aircraft Designed for Sonic-Boom Alleviation," AIAA Paper 2004-4846, Aug. 2004.

[15] Mack, R. J., and Kuhn, N., "Determination of Extrapolation Distance with Measured Pressure Signatures from Two Low-Boom Models," NASA TM-2004-213264, July 2004.

[16] Thomas, C., "Extrapolation of Sonic Boom Pressure Signatures by the Waveform Parameter Method," NASA TN D-6832, June 1972.

[17] Plotkin, K. J., "PCBoom3 Sonic Boom Prediction Model—Version 1.0c," Wyle Research Labs., Rept. AFRL-HE-WP-TR-2001-0155, Arlington,VA, May 1996.